RSC Advances

PAPER

View Article Online
View Journal | View Issue

Cite this: *RSC Adv.*, 2023, **13**, 14863

Preparation and properties of composite manganese/fluorine coatings on metallic titanium

Quanming Zhao,[a] Jieshi Wu,[b] Sujiajun Zhang,[b] Xiaohui Ni,[c] Bo Wang,[a] Kaihang Lu,[a] Pengpeng Zhang[a] and Ruisheng Xu *[b]

Titanium is widely used in implants because of its good mechanical properties and biocompatibility. However, titanium has no biological activity and is prone to causing implant failure after implantation. In this study, we prepared a manganese- and fluorine-doped titanium dioxide coating on a titanium surface by microarc oxidation technology. The surface characteristics of the coating were evaluated by field emission scanning electron microscopy, X-ray diffraction, X-ray photoelectron spectroscopy, and atomic force microscopy and profiler, and the corrosion resistance and wear resistance of the coating were also evaluated. The bioactivity of the coating on bone marrow mesenchymal stem cells was evaluated by *in vitro* cell experiments, and the antibacterial properties of the coating were evaluated by *in vitro* bacterial experiments. The results confirmed that the manganese- and fluorine-doped titanium dioxide coating was successfully prepared on the titanium surface, and manganese and fluorine were successfully introduced into the coating. The doping of manganese and fluorine did not change the surface morphology of the coating, and the coating had good corrosion resistance and wear resistance. The results of the *in vitro* cell experiment showed that the titanium dioxide coating with manganese and fluoride could promote the proliferation, differentiation and mineralization of bone marrow mesenchymal stem cells. The results of the bacterial experiment *in vitro* showed that the coating material could inhibit the propagation of *Staphylococcus aureus* and had a good antibacterial effect. Conclusion: it is feasible to prepare a manganese- and fluorine-doped titanium dioxide coating on titanium surfaces by microarc oxidation. The coating not only has good surface characteristics but also has good bone-promoting and antibacterial properties and has potential for clinical application.

Received 13th March 2023
Accepted 9th May 2023

DOI: 10.1039/d3ra01632c

rsc.li/rsc-advances

1. Introduction

Titanium (Ti) and its alloys have sufficient strength, toughness and good biocompatibility, so they are commonly used biomedical metal materials for repairing and replacing hard tissues (teeth and bones) in the clinic. However, titanium and titanium alloys are biologically inert materials, and their structures and properties are quite different from those of bone tissue. Generally, they cannot be chemically bonded to bone tissue like bioactive materials but are mechanically locked. Therefore, they do not significantly promote the healing of human bone tissue, which affects the clinical application of titanium implants.[1] To solve the above problems, researchers have performed much research work on the bioactive modification of titanium surfaces.

Various titanium surface modification technologies have been widely used. These technologies endow the material surface with some special properties by changing the chemical composition and structure of the titanium surface. Common methods include plasma spraying, chemical vapor deposition, ion implantation, the sol gel process, anodic oxidation and microarc oxidation.[2–6] Plasma spraying is the most widely used surface modification technology in the clinic. It uses a plasma arc as a heat source to heat some materials, such as alloys, ceramics and metals, to a molten or semimolten state and spray them at a high speed to the pretreated substrate surface to form a firmly attached coating. This technology has the characteristics of high efficiency, uniform coating, good repeatability and suitability for industrial production. However, plasma spraying has many shortcomings, such as it being a linear process, and it is difficult to form a uniform coating on the surface of porous or complex materials. When the temperature is high during the preparation of the coating, there will be high residual stress at the interface between the substrate and the coating during cooling. The high temperature process of plasma spraying easily decomposes hydroxyapatite (HA), resulting in impurities in the coating and low crystallinity of HA. High purity HA

[a]*Department of Orthopaedics, Guizhou Provincial People's Hospital, Guiyang 550002, Guizhou, China*
[b]*Department of Orthopaedics, Affiliated Hospital of Jiangnan University, Wuxi 214000, Jiangsu, China. E-mail: 9862018042@jiangnan.edu.cn*
[c]*Department of Orthopedics, Dafeng People's Hospital, Yancheng, Jiangsu 224100, China*

powder is used as raw material, which is expensive.[7] Similar to plasma spraying, other surface modification technologies also have their own advantages and disadvantages.

Microarc oxidation (MAO), also known as plasma electrolytic oxidation, is a new titanium surface modification technology that has been well developed in recent years. The technology involves putting titanium and its alloys in electrolyte aqueous solution, using electrochemical methods, and growing a layer of dense oxide film on the surface *in situ* under the combined action of thermochemistry, electrochemistry and plasma chemistry. The microarc oxidation product is a porous ceramic coating with good bonding strength to the substrate. The characteristics of the film are related to the time, voltage, current and other parameters of the microarc oxidation treatment, the mix ratio of the electrolyte, and the concentration of the electrolyte, among other factors. After microarc oxidation treatment, the wear resistance and corrosion resistance are significantly improved compared with those of matrix materials.[8] Compared with the existing surface treatment technology, microarc oxidation treatment technology has a series of advantages, such as high efficiency, simple processing, easy control of film thickness, low environmental pollution, *in situ* growth on the substrate surface, and high bonding strength with the substrate, and is an ideal surface treatment technology.

The biggest advantage of microarc oxidation is that it can introduce bioactive elements such as bone-promoting or antibacterial elements into the titanium surface and induce bone formation through the slow release of these bioactive elements. Zhou and Zhao[9] introduced different concentrations of cobalt onto the titanium surface through microarc oxidation. *In vitro* studies show that microarc oxidation with cobalt leads to good osteogenic and angiogenic activity. Huang *et al.*[10] used microarc oxidation technology to introduce copper into microporous coatings, and the results showed that the coating can enhance the osteogenesis and bactericidal ability mediated by macrophages. Zhang *et al.*[11] prepared a silicon-doped titanium dioxide coating, which improved the adhesion of MC3T3-E1 on a titanium surface. In addition, the coating prepared by microarc oxidation is rough and porous, so it has excellent bone induction performance. Proper roughness can increase the specific surface area and the area where osteoblasts adhere and grow on the surface. The porous structure of the microarc oxidation coating is similar to the structure of bone tissue. A similar structure can induce bone tissue regeneration. At the same time, the rough surface increases the contact area between the bone tissue and implant so that the bone tissue and implant can achieve mechanical locking and improve the stability of the implant. This rough, porous structure can also absorb calcium (Ca) and (P) elements in the electrolyte and form hydroxyapatite on the surface. Hydroxyapatite is the main component of bone tissue, so microarc oxidation coating can also indirectly promote bone formation.[12]

Manganese (Mn) is distributed in various organs and tissues of the human body and is an essential trace element for the human body. Manganese can activate genes and is the coenzyme factor or activator of some enzymes in the body, and it thus plays an important role in maintaining human life activities.[13] Manganese has an important impact on human metabolism. Manganese plays an important role in the synthesis of chondroitin sulfate and protein. It is closely related to the tenacity and hardness of connective tissue and calcium and phosphorus metabolism. It is an important element necessary to maintain normal bone metabolism and ensure normal physiological metabolism of the human body. Manganese is involved in the synthesis and activation of many enzymes and is also a component of some metalloenzymes. Manganese is a cofactor of glycosyltransferase, which is necessary for the formation of healthy cartilage and bone. Therefore, manganese deficiency will lead to abnormal bone development. Recent studies have shown that manganese has good antibacterial properties.[14] Fluoride is another essential trace element for human life activities and plays an important role in the growth and development of the skeleton and the maintenance of the physiological structure and function of the skeleton. Fluoride can promote the proliferation of osteoblasts, increase the activity of alkaline phosphatase, promote the formation of new bone, reduce the rate of bone resorption, and accelerate the biological combination between the implant and the host bone.[15]

The combination of good biological activity (promoting bone formation and antibacterial properties) and excellent surface structure is currently a hot topic in the research of titanium implants. Manganese and fluorine (F) are essential trace elements for the human body. Porous coatings containing manganese or fluorine were prepared using micro arc oxidation technology to enhance the biological activity of titanium implants, and there have been no literature reports so far. In this study, microarc oxidation technology will be used to prepare a manganese fluoride codoped TiO_2 biological coating on the surface of pure titanium. To evaluate in detail the surface characteristics, corrosion resistance and wear resistance of the coating, its activity and antibacterial performance against osteoblasts will be studied through *in vitro* experiments. Through this study, we hope to provide a new idea and method for the clinical application of titanium implants, with potential clinical application value.

2. Materials and methods

2.1 Preparation and characterization of specimens

A titanium rod was cut and processed into a round piece with a diameter of 14.6 mm and a thickness of 1 mm. Sandpaper of different mesh sizes was used to polish samples step by step, and then ultrasonic cleaning with acetone, absolute ethanol and deionized water were used in turn. Finally, the samples were dried in the drying oven for standby.

The microarc oxidation power supply used in this study is MAO-600-11A. The microarc oxidation time was set to 5 min, and the frequency was set to 1000 Hz. During the experiment, the electrolyte temperature was always maintained below 30 °C. After the completing the microarc oxidation, we rinsed the samples with deionized water for 5 minutes to remove impurities from the sample surfaces. Then, the samples were naturally dried in air for further experimentation.

Table 1 Electrolyte components of different samples

	Aqueous electrolyte concentration (mol L^{-1})			
Sample	Calcium acetate	Calcium glycerophosphate	Manganese acetate	Sodium fluoride
PT	—	—	—	—
MCP	0.2	0.02	—	—
MCP-MF	0.2	0.02	0.05	0.05

Grouping of test samples: PT is a blank control group. The basic electrolyte solution was prepared by dissolving calcium acetate and calcium glycerophosphate in deionized water. The sample after PT microarc oxidation in the basic electrolyte is marked as MCP, and the sample after microarc oxidation after adding manganese acetate and sodium fluoride to the basic electrolyte solution is marked as MCP-MF. The composition of different coating electrolytes is shown in Table 1.

The surface morphology of different materials was observed by field emission scanning electron microscopy (FE-SEM) equipped with an energy dispersive X-ray spectrometer (EDS) operating at 20 kV. The surface phases of the coating were analyzed by X-ray diffraction (XRD) using a Cu Kα irradiation in the regular range of $2\theta = 10–80°$ with an accelerating voltage of 40 kV, a current of 100 mA and a scanning speed of 5° min^{-1}. The elements and chemical composition of the coatings were analyzed by X-ray photoelectron spectroscopy (XPS) under the conditions of working voltage 2 kV, current 2 μA, oblique angle 45° and spot diameter 500 μm. Assessment of coating roughness by atomic force microscopy (AFM) in tapping mode with a scan size of 20 μm × 20 μm and profiler.

2.2 Manganese ion release experiment

The MCP-MF group samples were immersed in PBS solution, stored in a 37 °C incubator for 1 day, 3 days, 7 days, 15 days and 21 days after sealing, and then removed. The test was repeated for each group of samples three times. The concentration of manganese fluoride ions in the MCP-MF solution was detected with inductively coupled plasma-mass spectrometry (ICP-MS).

2.3 Corrosion resistance

The corrosion resistance was tested with an electrochemical test system (Shanghai Chenhua CHI760E electrochemical workstation) to test the Nyquist curve. A three electrode system was adopted, with a saturated calomel electrode (SCE) as the reference electrode (RE), a platinum electrode as the auxiliary electrode (CE), and the workpiece as the working electrode. The corrosion solution was 0.9 wt% NaCl. The sample was immersed in 30 mL of corrosion solution, stabilized for 60 min, and then impedance measurements were conducted. When measuring the polarization curve, the scanning speed was 1 mV s^{-1}.[16]

2.4 Abrasion resistance evaluation

Friction and wear tests of the PT, MCP and MCP-MF samples were carried out. The round-trip friction function of the nanomechanical property testing system of the British MML company is adopted. The load was 50 mN, the 5 Hz test lasted for 10 minutes, and the stroke length was 3 mm. The sample was soaked in a simulated body fluid (PBS) environment for 30 minutes, and the test was conducted in the presence of liquid.

The Brook Contour GT white light interference three-dimensional profiler was used to measure the width and depth of the wear scar to calculate the wear volume (W_v). The calculation formula is shown in eqn (1) and (2):

$$W_v = \frac{Lh}{6b}\left(3h^2 + 4b^2\right) \quad (1)$$

$$K = \frac{W_v}{PS} \quad (2)$$

where W_v is the wear volume (mm^3), L is the wear scar length (mm), h is the wear scar depth (mm), and b is the wear scar width (mm).

2.5 *In vitro* cell research

2.5.1 Isolation and culture of BMSCs. The studies involving animals were reviewed and approved by the Ethics Committees of Guizhou Provincial People's Hospital. BMSCs of rats were obtained by the whole bone marrow adherence method.[17] After SD rats were anesthetized, they were soaked and sterilized with 75% ethanol. The bilateral femurs and tibias of SD rats were extracted. The surrounding soft tissues were removed. The diaphysis ends were cut open. Ten milliliters of culture solution containing 10% fetal bovine serum was extracted with a syringe to wash the bone marrow cavity. The solution was collected into a centrifuge tube. After repeated tapping and mixing, it was inoculated into a 10 cm culture dish. The solution was placed in a 37 °C, 5% CO_2, 95% relative humidity incubator for culture. The solution was changed for the first time 48 hours later. After the adherent cells proliferated to approximately 70–80% confluence, they were subcultured with 0.25% trypsin, and second- to third-generation cells were used for subsequent studies.

2.5.2 Cytocompatibility evaluation. BMSCs were inoculated on the surface of each group of samples at a density of 2×10^4 per well and cultured in a 37 °C, 5% CO_2 constant temperature incubator for 3 days. The cells were assessed using a live/dead vitality/cytotoxicity kit and observed and photographed under a fluorescence microscope.

2.5.3 Proliferation of cells. The cell inoculation density and culture method were the same as above. After 3 days of culture, 200 μL of 50 μM EdU medium was added, and the samples were

incubated for 2 hours. Then, 100 μL of cell fixative was added to each well for 30 minutes at room temperature, and then 100 μL of *L* glycine was added. Next, 200 μL of 1× Apollo @ dye reaction solution was added for 30 minutes, followed by the addition of 200 μL of Hoechst 3342 reaction solution. Samples were then washed with PBS and assessed *via* laser confocal microscopy.

2.5.4 ALP staining. The cell culture method and inoculation density were the same as above. The culture was terminated on the 7th day after inoculation and fixed after washing with PBS. The osteoblast ALP was stained according to the BCIP/NBT kit, and the stereomicroscope was used to image.

2.5.5 Alizarin red staining for mineralization. The mineralization level of osteoblasts on the surface of different samples was evaluated with alizarin. The cell inoculation density and culture method were the same as above. The culture was terminated on the 14th day after inoculation, washed with distilled water and fixed with glutaraldehyde. Then, alizarin dye solution was added, and the samples were incubated at 37 °C for 30 minutes. The samples were then thoroughly cleaned with distilled water and imaged with a stereomicroscope.

2.6 *In vitro* antibacterial activity

2.6.1 Bacterial recovery and culture. *Staphylococcus aureus (S. aureus), which is typical bacteria infected with orthopedic implants,* was selected to test antibacterial activity. The bacteria were transferred to flat solid nutrient ager plate and cultured at 37 °C for 24 h, and the activated bacteria were inoculated into the prepared liquid medium and cultured at 37 °C overnight. A bacterial solution with a concentration of 10^5 cfu ml^{-1} of diluent was used as the bacterial solution for the experiment.

2.6.2 Fluorescence staining. Fluorescence staining was used to evaluate the survival and death of bacteria on the surface of each group of samples. After the bacteria were cultured on the surface of the samples for 24 hours, they were gently rinsed with PBS, and 50% of them were taken. The mixture of acridine orange (AO)/propidium iodide (PI) 1 : 1 dye was evenly dropped on the surface of the sample and dyed in the dark for 10 minutes. The survival of bacteria on the surface was observed under inverted fluorescence microscopy.

2.7 Statistical analysis

All data are expressed as the mean ± standard deviation and were analyzed by SPSS 18.0 software. One-way ANOVA and the SNK test were used to compare the differences between groups. $P < 0.05$ indicates a significant difference.

3. Results

3.1 Surface morphology of different specimens

Fig. 1 shows the surface morphology of each group of samples as imaged by SEM. The surface of the PT group is smooth, while that of the MCT group is porous, with different sizes of holes and irregular shapes. The pore size is approximately 2–8 μm. The MCT-MF group and MCT group are similar, and the surface is covered with irregular micropores of different sizes.

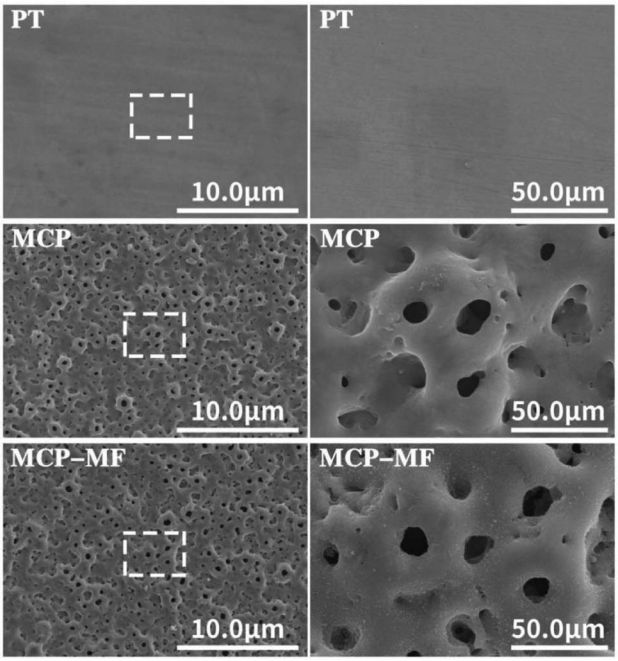

Fig. 1 SEM surface morphology of different samples under low and high magnification (×600 and ×3000). The plasma oxidation time is 5 min, and the reaction temperature is room temperature.

Fig. 2 shows the morphology of the cross section of MCT-MF as imaged by SEM. From right to left, it is titanium matrix, coating and resin. We can clearly see that the coating is criss-crossed and has no obvious boundary with the substrate, so it can be seen that the coating is firmly bonded with the substrate.

Fig. 3 shows the surface morphology of each group of samples measured by AFM. Compared with the smooth and flat PT surface, after microarc oxidation, the material surface exhibits pore-like structures of different sizes. The 3D image is more intuitive, and many crater-like structures appear on the surface of the coating. After microarc oxidation of the PT surface roughness, the micron-level roughness of its coating increases. Compared with the MCT group, the doping of manganese and fluorine does not change the morphology and roughness of the material. This shows that the addition of manganese and fluorine has little effect on the roughness of the MAO coating.

Fig. 4 shows the mapping diagram of MCT-MF. It is clear from the mixed element diagram that MCT-MF consists of titanium, calcium, phosphorus, oxygen, manganese and fluorine elements, in which titanium comes from the matrix, and calcium, phosphorus, manganese and fluorine come from the electrolyte solution. It is also clear that manganese and fluorine are successfully incorporated into the microarc oxidation microporous coating. It can be further seen from the mapping diagram of MCT-MF that, like calcium, phosphorus and oxygen, manganese and fluorine are evenly distributed on the surface and inside the pores of the coating.

Fig. 5 shows the profiler surface topographies determined for each group of samples. The surface roughness distributions

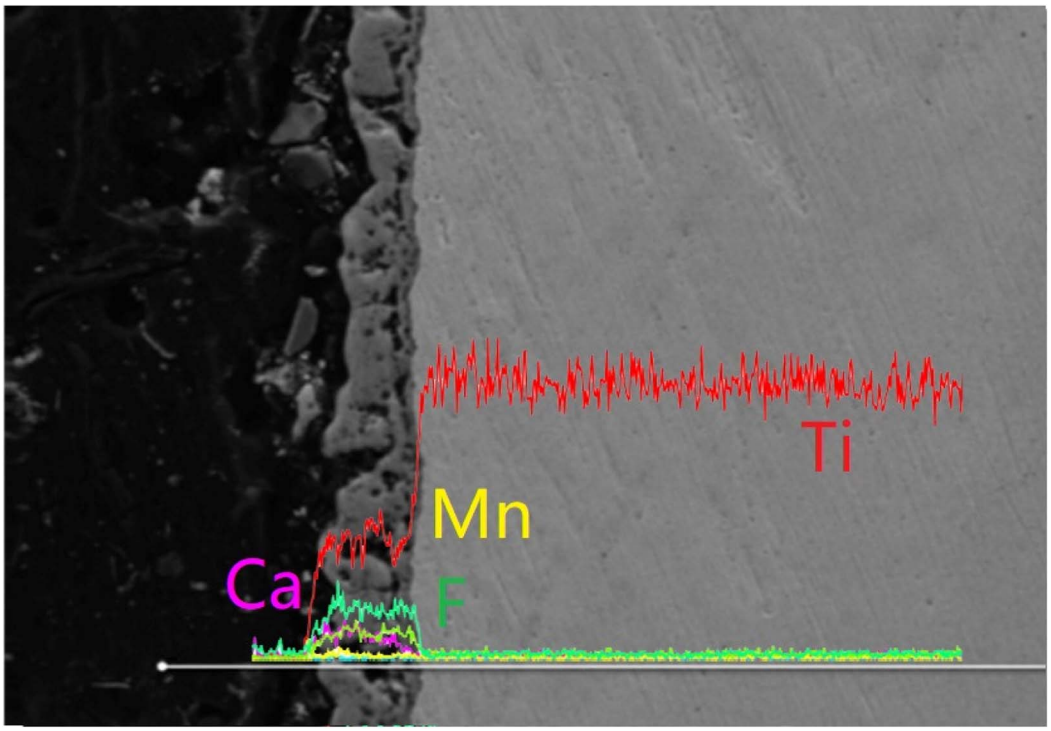

Fig. 2 SEM cross section morphology of MCT-MF (From right to left, it is titanium matrix, coating and resin.).

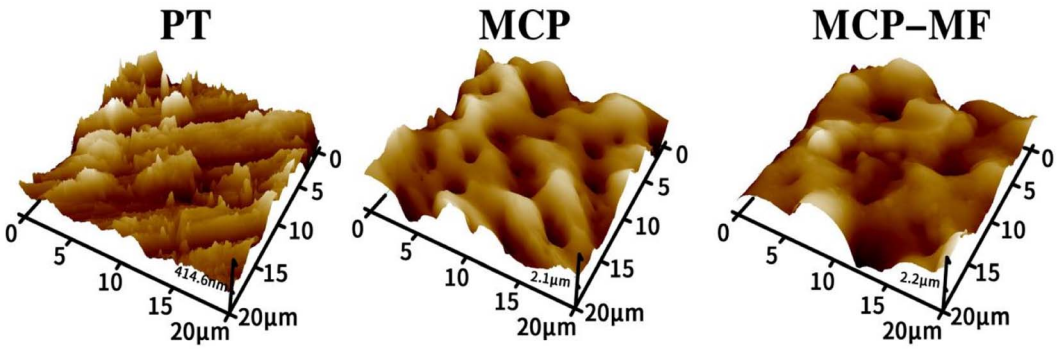

Fig. 3 AFM surface topographies of different samples.

for each group of samples were uniform, and the MCP and MCP-FM samples showed volcano-like multilevel pore-void structures. Further quantitative analyses of the surface roughness values showed a PT Ra of 254.02 ± 23.58, a MCP Ra of 894.50 ± 16.93 and a MCP-FM Ra of 1079.14 ± 17.6. The roughness for each group of samples conformed to this trend and decreased in the order MCP > MCP-FM > PT. MCP-FM increased the surface roughness of the Ti after plasma oxidation.

Fig. 6 shows the combination diagram of the X-ray diffraction peaks of each group of samples. It is clear that PT is composed of titanium peaks, and the MCT and MCT-MF samples are mainly composed of characteristic peaks of rutile and anatase titanium dioxide, except for titanium peaks. There is no peak of manganese and fluorine in the MCT-MF sample. It is considered that the content of manganese and fluorine in the coating is small or manganese and fluorine exist in an amorphous form.

Fig. 7 shows the full spectrum of X-ray photoelectron spectroscopy of MCT-MF, which is consistent with the results of mapping. MCT-MF is composed of titanium, oxygen, calcium, phosphorus, manganese and fluorine. The peak in the Ti2p spectrum corresponds to TiO_2, the Ca2p peaks are at 347.8 eV and 351.2 eV, and the P2P peak is at 133.4 eV, which indicates that Ca2p and P2P exist in the form of calcium phosphate. The peaks of Mn2p are located at 641.8 eV and 653.7 eV, corresponding to Mn_2O_3,[18] and the binding energy corresponding to the peak position of F1s is 685.2 eV, indicating that the F

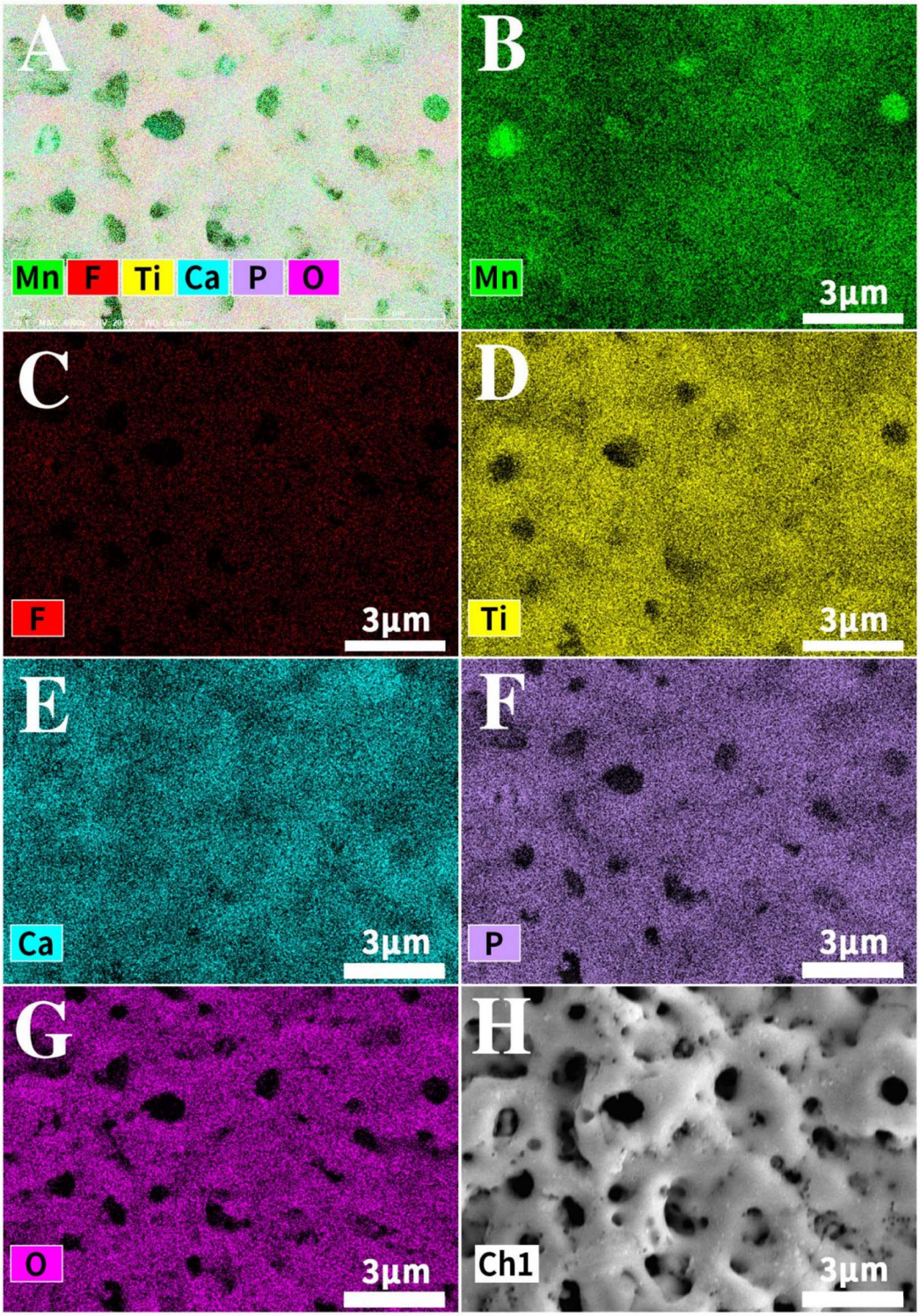

Fig. 4 EDS mapping image of the MCT-MF. (A) Composite map of MCT-MF, (B) Mn, (C) F, (D) Ti, (E) Ca, (F) P, (G) O and (H) surface morphology.

element in the coating exists in the form of calcium fluoride.[19] In the O1s spectrogram, there are four characteristic peaks: the peak at 533.0 eV corresponds to the binding energy of manganese trioxide, the peak at 531.2 eV corresponds to the binding energy of oxygen in phosphate, and the peak at 530.0 eV corresponds to the binding energy of oxygen in TiO_2.

3.2 Corrosion resistance

Fig. 8 shows the Nyquist plots of each group of samples. To compare the corrosion resistance of the samples, electrochemical impedance spectroscopy (EIS) of PT, MCP and MCP-MF was measured under the self-corrosion potential. It can be

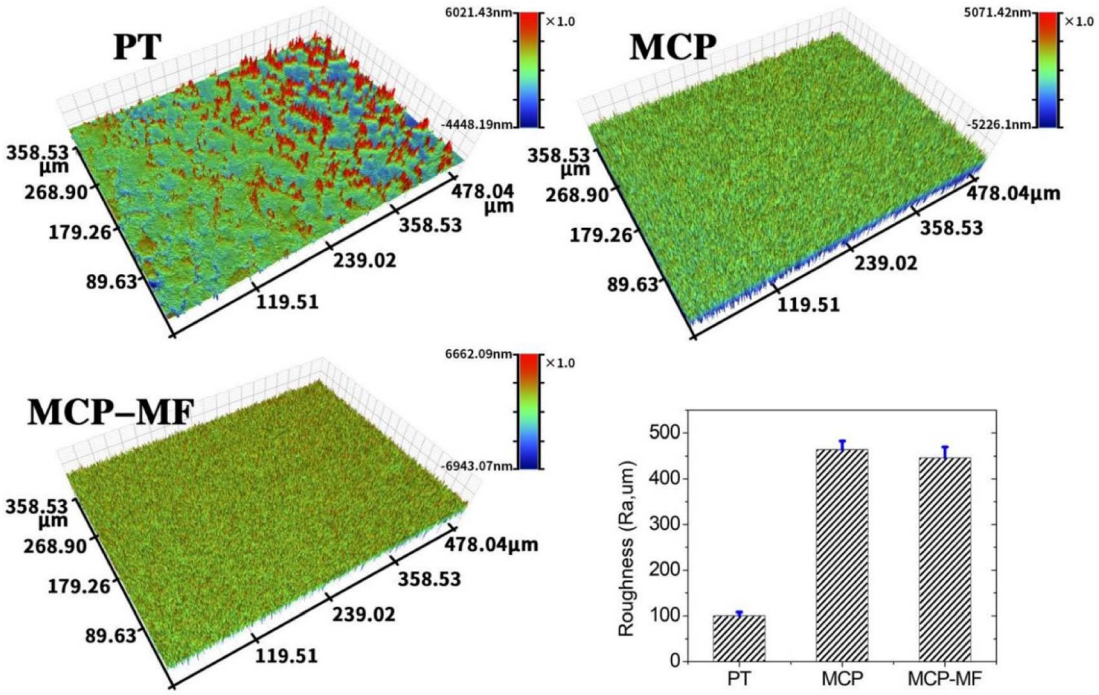

Fig. 5 Profiler surface topographies different samples, and (A) PT, (B) MCP and (C) MCP-FM.

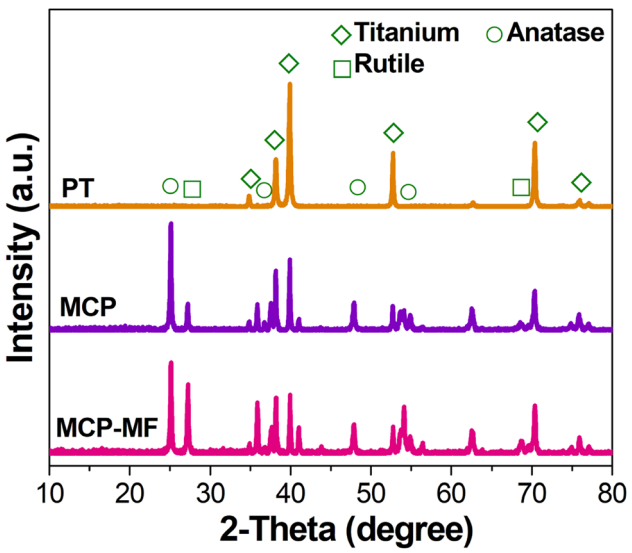

Fig. 6 Combination diagram of the X-ray diffraction peaks of different samples.

clearly seen that the impedance shapes of the three samples are basically the same, showing a capacitive arc. The capacitive arc diameter of PT, MCP and MCP-MF gradually increases, and the capacitive arc diameter of MCP-MF is significantly larger than that of the other two samples, showing good corrosion resistance.

3.3 Manganese ion slow release

Fig. 9 shows the cumulative release curves of manganese and Ca of the MCT-MF samples after immersion in a-MEM of different durations. In this study, the release of Manganese and Ca ions in MCT-MF samples at different time points was detected by ICP–MS. It is clear that with increasing time, manganese and Ca ions are released slowly in a-MEM solution. Fig. 9(a) shows the slow release curve of manganese ions. We can see that manganese ions are released rapidly in the first 7 days, reach a peak on the 7th day, and then release slowly. Fig. 9(b) shows the slow release curve of Ca ions. Similar to manganese ions, it reaches a peak on the 7th day and then releases steadily.

3.4 Friction resistance

The wear resistance of the material is expressed by the wear amount. The depth and width of the wear scar are measured by a white light interferometer, and then the wear volume W_v and wear rate K are calculated. According to the results of wear volume W_v and wear rate K, the wear resistance of the MCP and MCP-MF samples is considerably better than that of the PT samples. The wear resistance of each group of materials conforms to the following trend: MCP-MF > MCP > PT, which demonstrates that MCP-MF has good wear resistance (Table 2).

Fig. 10 shows the SEM images of the wear scar morphology of PT, MCP and MCP-MF. In this study, the scratch depth of each group of samples was observed by SEM. It is clear that the scratches on the PT surface are deep, indicating serious wear, while the scratches on the MCP and MCP-MF samples are shallow, demonstrating good wear resistance.

3.5 Cytocompatibility evaluation

Fig. 11 shows the results of live/dead staining of BMSCs cultured on different samples for 3 days. Although there were a small number of red dead cells in each group, the samples

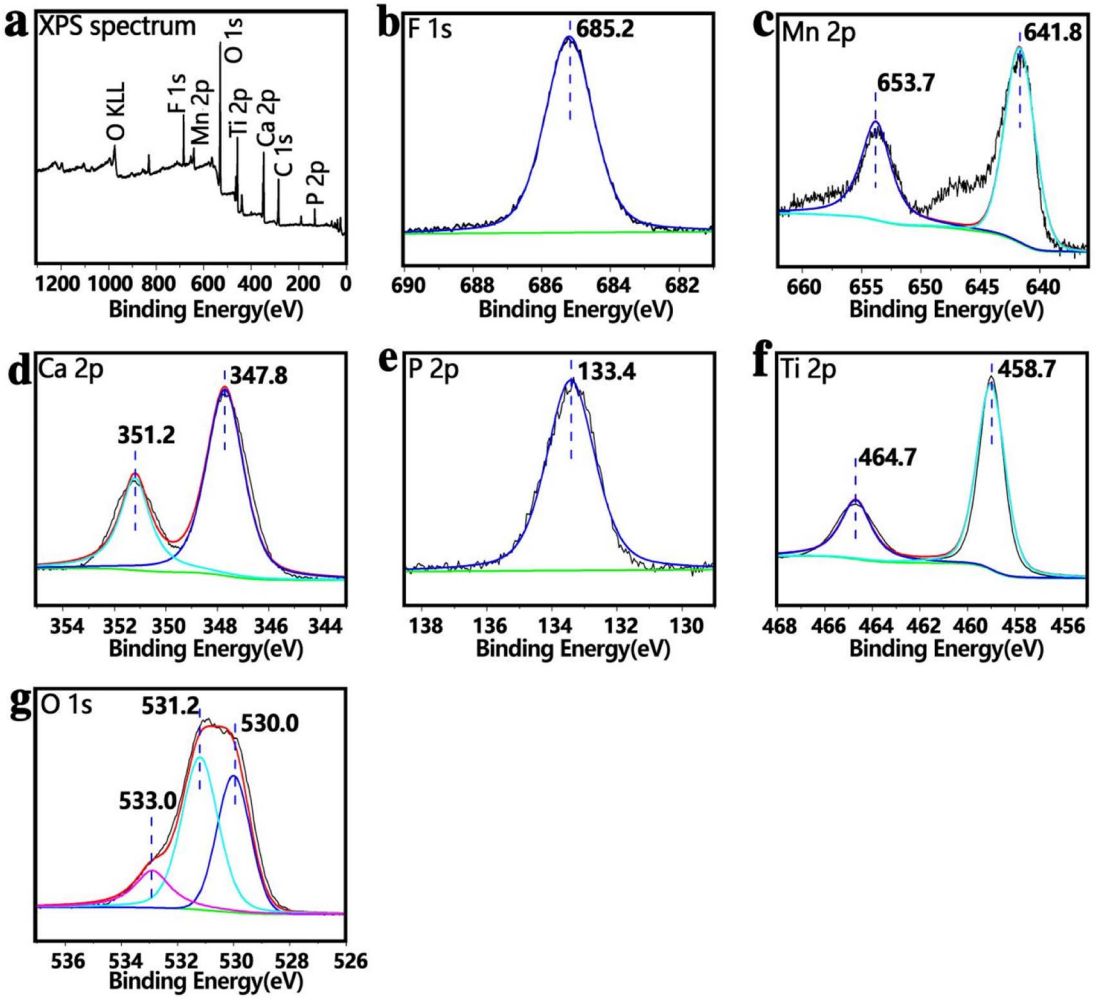

Fig. 7 X-ray photoelectron spectroscopy spectra of MCT-MF. (a) Complete XPS spectrum, (b) F1s, (c) Mn2p, (d) Ca2p, (e) P2p, (f) Ti2p, and (g) O1s spectra.

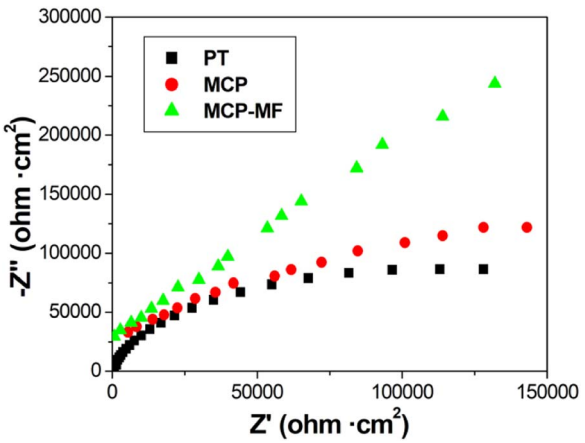

Fig. 8 Nyquist plots of EIS data of PT, MCP and MCP-MF in 0.9 wt% NaCl solution.

were generally occupied by green living cells, and there was no significant difference between groups, indicating that MCP-MF has no obvious cytotoxicity and has good biocompatibility.

3.6 Cell activity evaluation

In this study, EdU staining was used to evaluate the proliferation of BMSCs in each group of samples. Fig. 12 shows the cell proliferation results of BMSCs cultured on different sample surfaces for 12 hours. The red fluorescence-labeled cells are EdU-positive. The proliferation of samples in each group was basically in the following order: MCP-MF > MCP > PT. The proliferation rate of the MCP-MF group was significantly higher than that of the Ti group, suggesting that manganese and fluoride ions in MCP-MF play a key role in cell proliferation.

Fig. 13 shows the ALP staining results of BMSCs cultured on different sample surfaces for 7 days. Compared with the PT group and MCP group, the surface staining of the MCP-MF group was deeper, and the quantitative results further confirmed that the ALP staining of samples in each group was in line with the following trend: MCP-MF > MCP > PT. It can be inferred that the doping of manganese and fluoride promoted the differentiation of BMSCs.

Fig. 14 shows the ECM mineralization results of BMSCs cultured on different samples for 14 days. Mineralized nodules can be seen on the surface of each group of samples. Compared

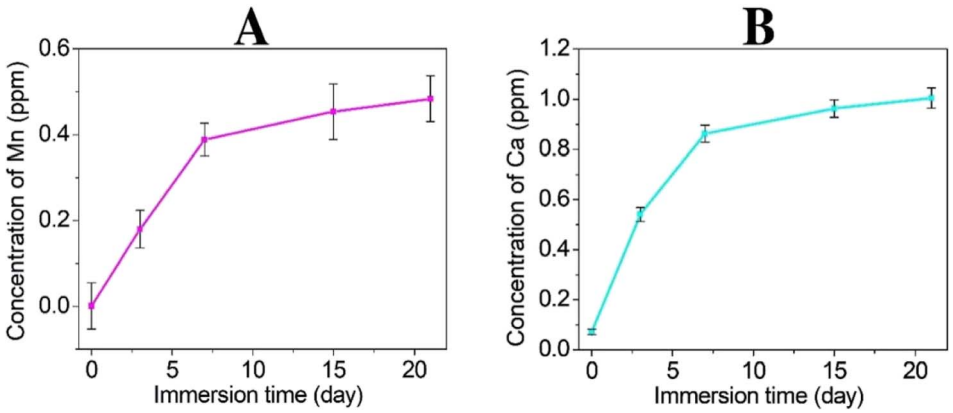

Fig. 9 Cumulative release curves of Mn (A) and Ca (B) of the MCT-MF samples after immersion in a-MEM of different durations.

Table 2 Wear volume W_v and wear rate K of different samples

Sample	W_v	K
PT	9.232×10^{-5}	0.739
MCP	5.186×10^{-5}	0.415
MCP-MF	4.469×10^{-5}	0.358

with the PT group and MCP group, the number of mineralized nodules in the MCP-MF group was greater, and the degree of surface mineralization was higher. The quantitative map is further clarified. The mineralization of samples in each group conforms to the following trend: MCP-MF > MCP > PT.

3.7 Antibacterial activity

Fig. 15 shows the fluorescent staining results of living and dead bacteria in different samples. Acridine orange (AO) can pass through living cells with intact cell membranes, combine with cell DNA, and emit green fluorescence. Propidine iodide (PI) can enter the interior of necrotic bacteria, combine with its DNA, and emit red fluorescence. The survival of bacteria on the coating surface can be directly defined by observing the

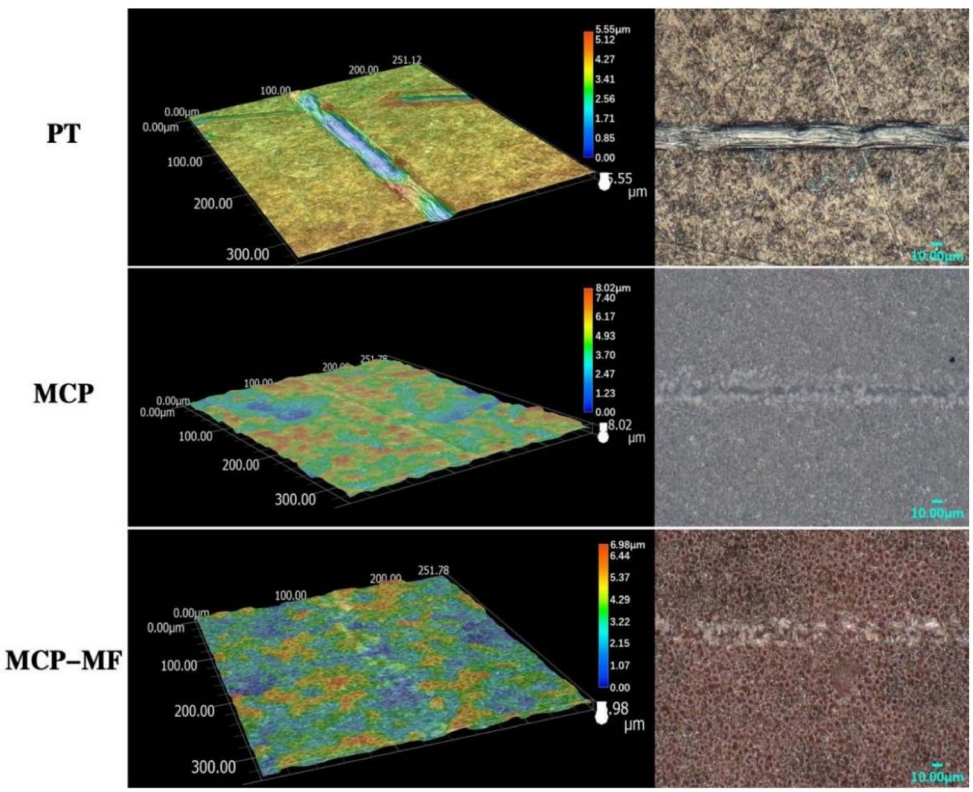

Fig. 10 SEM images of the wear scar morphology of PT, MCP and MCP-MF.

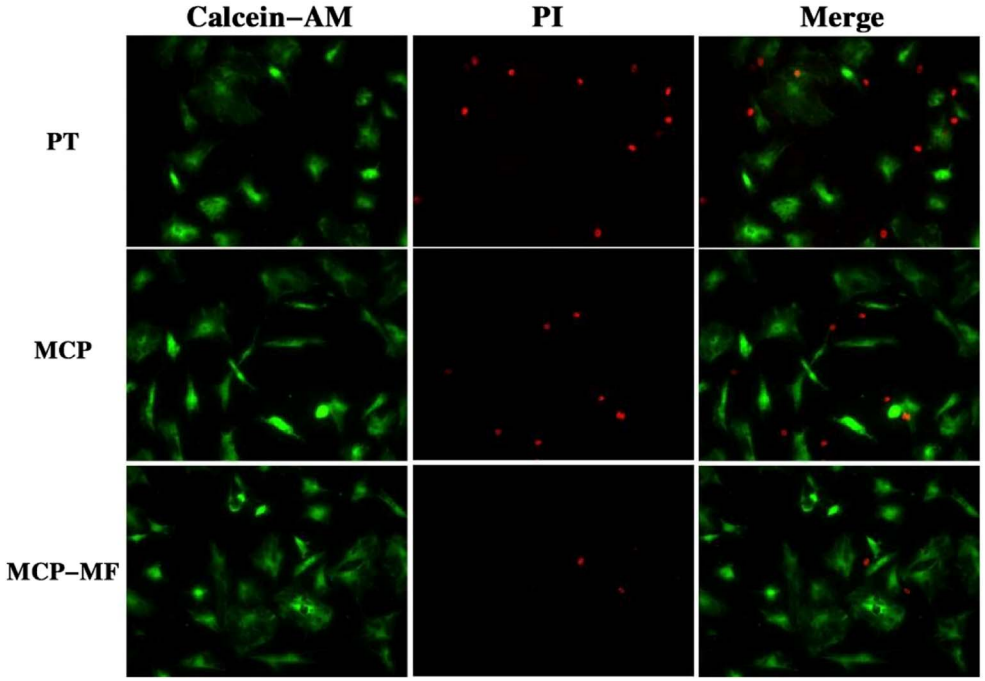

Fig. 11 Live (green)/dead (red) staining of cells incubated for 3 days on different samples.

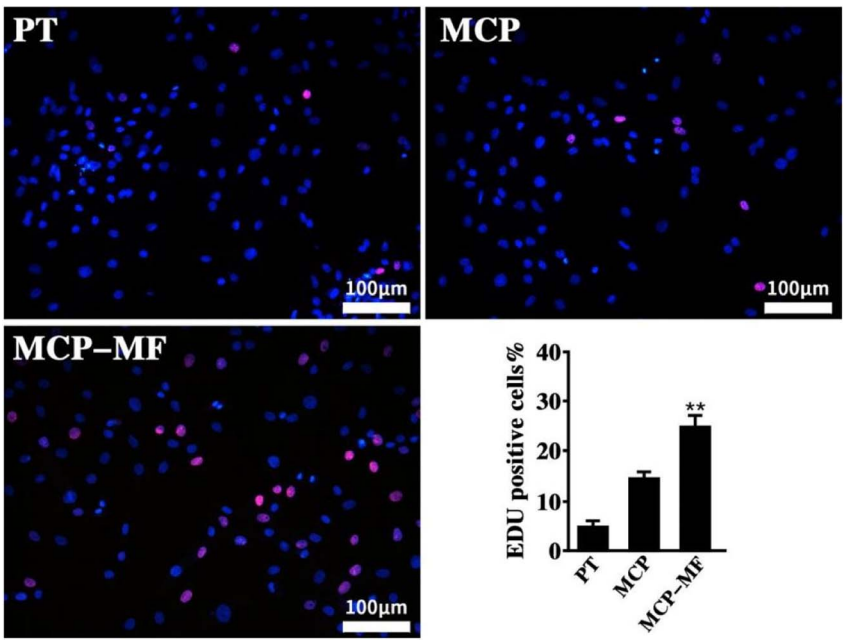

Fig. 12 5-Ethynyl-2′-deoxyuridine staining measured after 3 days of culture. Data represented mean ± SD (**p < 0.01 compared to PT group).

bacterial color after the interaction with the stain. It can be seen from the fluorescence images in Fig. 1 that the bacteria on the surface of the PT group samples are all alive after 24 hours of culture, indicating that PT has no antibacterial activity. There were many living bacteria on the surface of the MCP group, but there were significantly fewer than on the PT group. In the MCP-MF group, the red color on the surface of the sample accounts for the majority, which is the bacteria that disintegrate and die. This shows that MCP-MF has good antibacterial properties, and it can be inferred that the release of manganese and fluoride ions in the coating is responsible for the good antibacterial properties.

4. Discussion

Titanium and titanium alloys are widely used clinically in orthopedic implants because of their good mechanical properties, chemical stability and biocompatibility. However, the

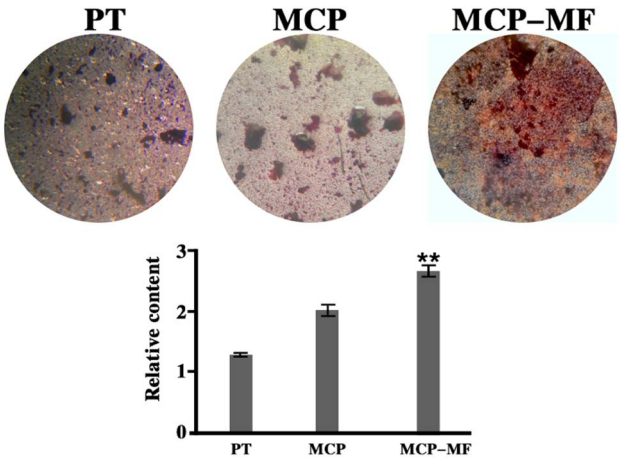

Fig. 13 Alkaline phosphatase staining of BMSCs after 7 days of culture. Data represented mean ± SD ($n = 3$) (**$p < 0.01$ compared to PT group).

biological inertness of the surface of titanium-based implants leads to poor integration with the surrounding bone tissue (osseointegration), which leads to aseptic loosening. In addition, titanium-based implants themselves lack antibacterial properties, which may easily lead to bacterial adhesion or even biofilm formation, leading to implant-related infections and, in serious cases, implant failure. Because bacterial adhesion, biofilm formation and cell adhesion bone integration occur on the surface of titanium implants, it is crucial for titanium-based implants to undergo surface modification to achieve excellent antibacterial ability and good bone integration performance, thus improving their long-term service.[20] Based on this, in this study, microarc oxidation was used to create a TiO_2 coating with both osteogenic and antibacterial properties on the titanium surface. The coating has a porous structure, and manganese and fluorine are uniformly distributed on the surface of the coating. The *in vitro* cell/bacterial experiments confirmed that the coating had good biological activity and facilitated the integration of the titanium implant surface structure.

The surface morphology and chemical composition of titanium implants are two important characteristics that affect bone integration,[21] and at present, research on implant surface modification mainly focuses on both. Micron roughness of the implant surface can improve the contact area between the material surface and body tissues, provide necessary space and microenvironment for the growth of cells and tissues and is conducive to the formation of extracellular matrix, the transport of nutrients, and the growth of nerves and blood vessels. There are many modification methods to form micron-level rough structures on implant surfaces, such as mechanical processing, acid etching, sand blasting, plasma spraying and microarc oxidation.[22,23] Among them, the microarc oxidation method can prepare a porous, micron-level rough titanium dioxide coating on the material surface. This coating is considered to improve the biocompatibility of titanium implants, reduce human rejection, and facilitate the adhesion and proliferation of osteoblasts on the material surface.[24] However, the simple surface morphology modification of materials cannot meet the requirements of bone formation after implantation. Adding bioactive elements *via* surface morphology modification is an effective means to further improve the osteogenic activity of titanium surfaces. Manganese and fluoride play an important role in maintaining bone health. They have osteoinductive activity and can promote the differentiation of osteoblasts. Manganese and fluoride ions are incorporated into the

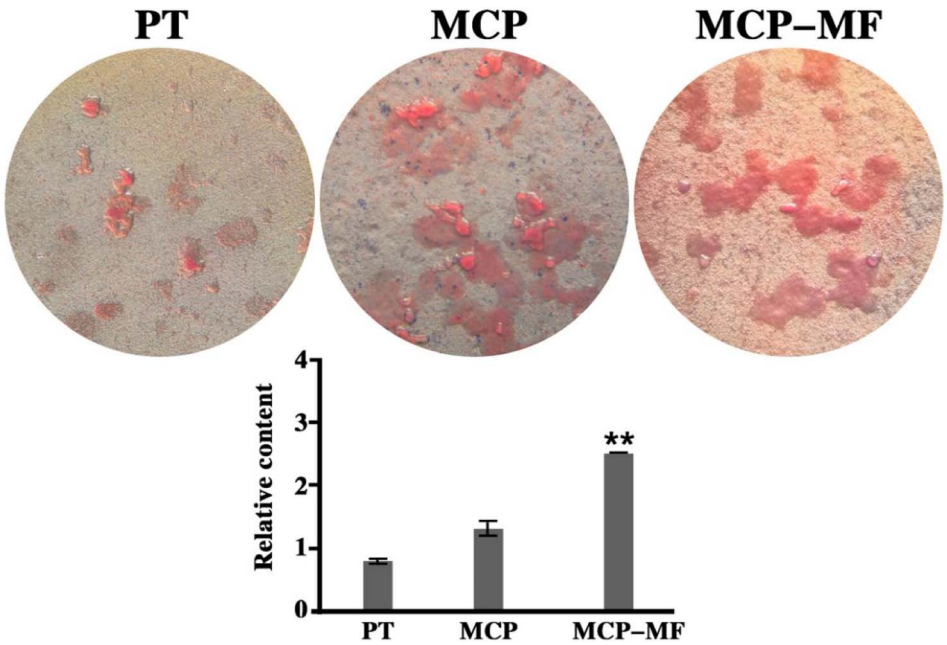

Fig. 14 Alizarin red staining for mineralization of BMSCs after 14 days of culture. Data represented mean ± SD ($n = 3$) (**$p < 0.01$ compared to PT group).

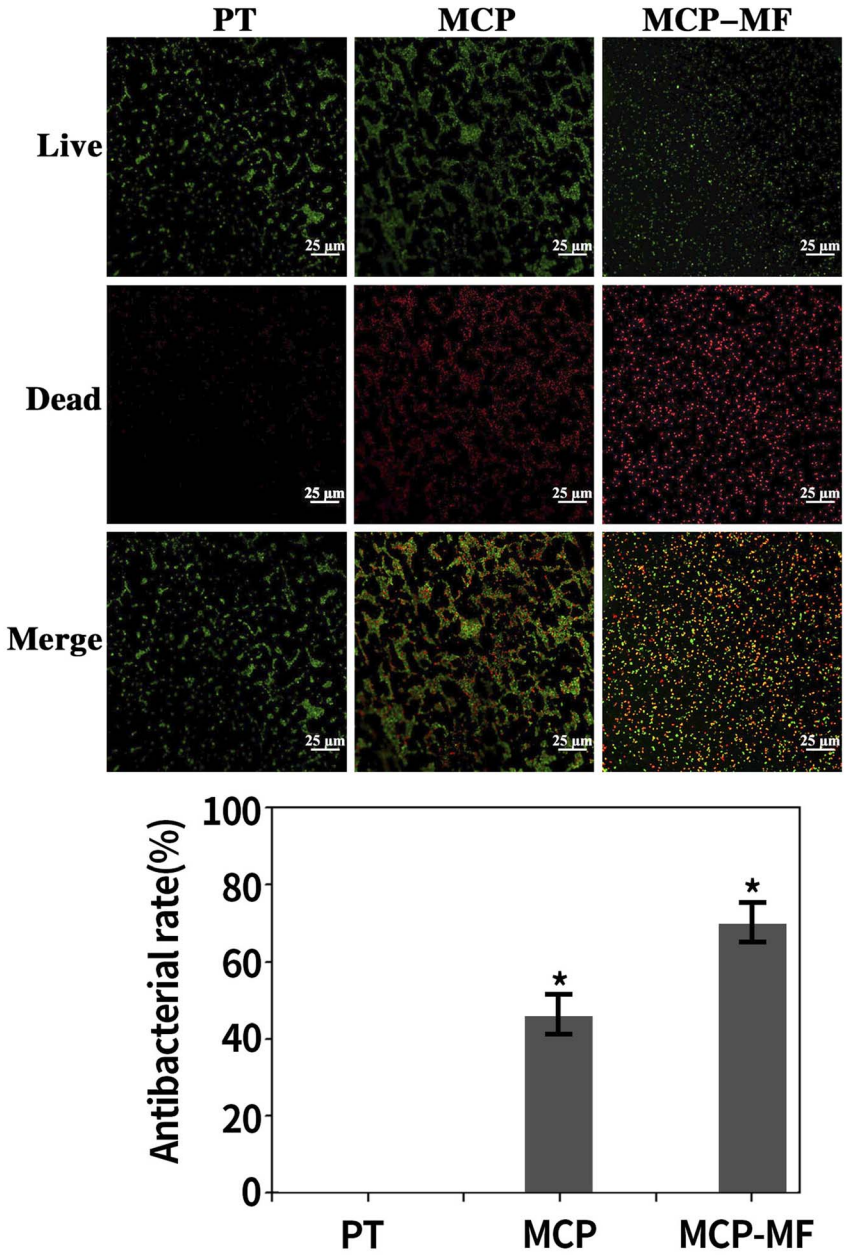

Fig. 15 Fluorescence staining results for live and dead bacteria in different samples. Data represented mean ± SD ($n = 3$) (*$p < 0.05$ compared to PT group).

bioactive coating by microarc oxidation technology, which is expected to combine the advantages of porous titanium dioxide coating and bioactive manganese and fluoride ions. Thus, the new magnesium-doped microarc oxidation coating to modify the titanium surface can improve the osteoinduction of titanium implants.

In this study, a composite oxidation film containing Mn, F, Ca and P was prepared on a titanium surface by microarc oxidation. The SEM test results show that the coating surface formed on the titanium surface after microarc oxidation treatment appears to be uniformly sanded, with holes of different sizes distributed around the holes in the form of volcanic hills, which are clear signs of sintering and melting, and these surface morphologies are consistent with those reported in the literature.[25] The research shows that these holes are plasma discharge channels in the microarc oxidation process. High temperature, high electric field and high voltage are formed in the process of partial discharge arcing on the titanium surface, and titanium dioxide and other substances are transformed into ceramic phase crystals under the action of high temperature.[26] In this study, the surface morphology of the MCP-MF group is consistent with that of the MCP group. However, the surface morphology of the MCP-MF group is considerably different from the grooved morphology of the blank control group PT group without microarc oxidation treatment in the same direction, which indicates that microarc oxidation has

changed the original morphology of the pure titanium surface and produced a porous structure on its surface. It has been proven in the literature that a rough, porous surface increases the surface area of the implant without changing the implant volume, which is conducive to the distribution of stress. On the porous surface, the cell adhesion rate is significantly higher than that on the machined surface and is conducive to the extension and proliferation of cells.

The surface roughness of materials has an inevitable relationship with the surface morphology of materials. It is generally believed that the rougher the surface, the larger the specific surface area, the better the hydrophilicity, and the more conducive to cell adhesion on the surface of materials. At present, the definition of implant surface roughness is not entirely consistent. Most studies regard average roughness Ra < 1 μm as smooth and Ra > 1 μm as rough.[27] In this experiment, the surface roughnesses of the MCP-MF and MCP group materials after microarc oxidation are characterized as rough surfaces. Because the mechanisms and factors of implant surface roughness that affect osteoblasts have not yet been clarified, there is no consensus on the appropriate roughness. Some studies have shown that an excessively smooth or directionally rough surface of implants is not conducive to cell adhesion and affects bone bonding ability. However, the irregular micron roughness can promote the adhesion and proliferation of osteoblasts and the activity of alkaline phosphatase, which is conducive to the mechanical chimerism of implants and bone tissue.[28] Moreover, the increase in roughness can increase the implant surface area and the mechanical locking force of potential bone growth into the implant surface, and the shape of the rough surface can also guide the tissue and guide the formation of bone in specific areas of the implant.

Adhesion is the first step for osteoblasts to contact the implant material. Only when cells adhere to the implant can implant bone become bonded, which is the basis for the success of the implant. Cell adhesion includes early adhesion of extracellular matrix proteins and late cell adhesion. The early adhesion of extracellular matrix proteins is a physical and chemical connection, which is mainly caused by the force between ions and van der Waals forces, so that proteins can be adsorbed on the surface of materials. Late cell adhesion is mediated by the interaction of multiple biological molecules and multiple signal transduction pathways. Only when cells effectively adhere to the surface of the implant can osteoblasts enter the subsequent stages of proliferation and differentiation. In addition, there is a competition mechanism between cells and bacteria. When cells can adhere to the surface of implant materials faster, bacteria are prevented from adhering to the surface of implant materials. Therefore, faster early cell adhesion can win the competition between the two, which is also of great significance to prevent implant-related infection. The effect of implants on osteoblast adhesion can be evaluated by checking the number of cells attached to the implant surface at the early stage of culture. It has been confirmed that micro arc oxidation coating can promote the adhesion of MC3T3-E1 cells, mainly due to the improvement of the roughness and wettability of titanium implants by microarc oxidation coating.[8]

When cells effectively adhere to the implant surface, they then enter the proliferation stage. The study of the effect of cell growth and proliferation on the surface of materials is important for evaluating the biocompatibility and bioactivity of implants. There are many factors affecting osteoblast proliferation activity, such as implant surface morphology, chemical element composition, surface hydrophilicity, surface charge, and disinfection method of the implant material surface.[29] In this study, we found that the proliferation rate of the MCP-MF group was significantly higher than that of the Ti group, and the difference was statistically significant, indicating that the manganese fluoride-doped titanium dioxide coating can promote the proliferation of BMSCs. The good biological activity of the manganese fluoride-doped titanium dioxide coating is related not only to the porous structure of the coating but also to the slow release of manganese fluoride ions from the coating. Yu *et al.*[30] introduced manganese ions into the titanium surface using plasma immersion ion implantation and deposition (PIII&D) technology, and further research found that the bioactive membrane has antibacterial and bone promoting effects. Zhao *et al.*[31] found that a coating containing copper and magnesium fluoride on a titanium surface has good biological activity.

The differentiation and mineralization of BMSCs are the basis of bone integration. The microarc oxidation coating can not only promote the early adhesion and proliferation of osteoblasts but also effectively promote the differentiation and mineralization of osteoblasts.[32] In the process of osteogenesis, each gene has unique expression characteristics at different time points through strict regulation of osteogenesis-related genes. Generally, bone formation is a complex and orderly process of protein and extracellular matrix synthesis that is regulated by a series of growth factors and expresses many related markers, such as alkaline phosphatase (ALP), type I collagen (Col-1) and runt-related transcription factor 2 (Runx2). Therefore, we can evaluate the osteogenic ability of the implants by detecting osteogenic differentiation- and mineralization-related proteins. In this study, we evaluated the differentiation and mineralization ability of the materials through ALP staining and alizarin staining. The results show that the titanium dioxide coating doped with manganese ions and fluoride ions is conducive to the differentiation and mineralization of BMSCs, which is similar to previous reports.[33]

In addition to the biological activity of cells, the evaluation of antibacterial performance is another important indicator of the biological activity of titanium implants. After implantation into the body, a layer of protein will quickly be adsorbed on the surface of the implant. Although this layer of protein is conducive to cell adhesion, it is also conducive to bacterial aggregation. If the bacterial colonization is successful, the bacteria will rapidly reproduce, gather and adhere to the surface of the material and finally form a bacterial biofilm. The existence of this biofilm will ensure that the internal bacteria will not be attacked by the host defense system and antibacterial agents through a variety of protection mechanisms, thus producing strong drug resistance. With the expansion of the biofilm, an inflammatory reaction will occur around the

implant, which will eventually lead to implant failure. Research shows that early prevention of bacterial biofilm formation is the most effective method to prevent inflammatory reactions around implants.[34] Some broad-spectrum antibiotics, such as vancomycin and amoxicillin, were loaded on the surface of the material to prepare a coating with antibacterial properties, but its disadvantages were limited drug loading and unsatisfactory release. Recent research has focused on metal elements silver, copper and zinc due to their broad-spectrum antibacterial ability and long-term antibacterial effect, and they have been proven to have good antibacterial performance in clinical applications.[35,36] In this study, the manganese fluoride-doped titanium dioxide coating was proven to have good antibacterial performance, indicating that the slow release of manganese ions and fluoride ions in the coating can inhibit the propagation of bacteria. Our research is consistent with previous literature reports.[37,38]

Implant materials must have good biocompatibility, and good biocompatibility first requires the material to be safe and nontoxic, so it is particularly important to evaluate the cytotoxicity of materials. Studies have found that when the content of a particular element exceeds a certain amount, it will produce corresponding cytotoxicity or cause related diseases. Although manganese is an essential trace element for the human body, when the intake of manganese in the human body exceeds the human absorption limit, it will lead to nervous system damage, such as movement retardation and stiffness, significantly reduced memory and speech disorders. Like manganese, excessive fluoride can cause fluorosis and skeletal fluorosis, which are manifested as joint stiffness, bone deformation, and symptoms and signs of nerve root and spinal cord compression.[39] In this study, we introduced a small amount of manganese and fluorine into a microarc oxidation coating through microarc oxidation technology and evaluated the cytotoxicity of the coating through live/dead cell staining. The results showed that the coating had good cell compatibility.

Although the manganese and titanium dioxide coatings prepared in this study have been proven through cell experiments and bacterial experiments to have good biological activity and antibacterial properties, there are still shortcomings, such as accounting for the complex microenvironment in the human body. Good *in vitro* experimental effects need to be verified by *in vivo* experiments. Whether this coating can promote bone bonding and bone regeneration of implants *in vivo* needs further research and verification. Therefore, we will conduct further relevant research through animal experiments in the future.

5. Conclusion

In this study, manganese and fluorine were doped into a titanium dioxide coating through microarc oxidation technology, and a manganese fluoride-doped TiO_2 coating was prepared. The coating not only has a good surface morphology but also has good wear resistance and corrosion resistance. *In vitro* studies show that the manganese- and fluoride-doped TiO_2 coating has good cell compatibility. More importantly, the coating can promote the proliferation and differentiation of BMSCs. In addition, the manganese- and fluoride-doped TiO_2 coating can inhibit the proliferation of *S. aureus* and has good antibacterial performance. This study provides a new way to improve the bioactivity of titanium and has potential in clinical application.

Ethical statement

All animal procedures were performed in accordance with the Guidelines for Care and Use of Laboratory Animals of Guizhou University and approved by the Animal Ethics Committee of Guizhou Provincial People's Hospital.

Conflicts of interest

There are no conflicts to declare.

Acknowledgements

This work was supported by Guizhou Provincial Science and Technology Projects (grant number ZK [2022] general 267), Key Research and Development (Key R&D) Plan of Jiangsu Province – social development (grant number BE2021683), East-West Collaborative Medical and Health Research Project of Haidong Science and Technology Bureau (grant number 2021-HDKJ-Y3), Guiyang Science and Technology Plan Project (grant number [2023] 48-23), Guizhou Provincial People's Hospital fund (grant numbers GZSYBS [2022] 01 and GZSYQN [2022] 03).

References

1 T. Xue, S. Attarilar, S. Liu, J. Liu, X. Song, L. Li, B. Zhao and Y. Tang, *Front. Bioeng. Biotechnol.*, 2020, **8**, 603072.
2 J. L. Ong, D. L. Carnes and K. Bessho, *Biomaterials*, 2004, **25**, 4601–4606.
3 J. Zhao, Y. Guo, A. Lan, W. Luo, X. Wang, L. Fu, Q. Cai and Y. Zhou, *J. Biomed. Mater. Res., Part A*, 2018, **106**, 265–271.
4 X. J. Wang, H. Y. Liu, X. Ren, H. Y. Sun, L. Y. Zhu, X. X. Ying, S. H. Hu, Z. W. Qiu, L. P. Wang, X. F. Wang and G. W. Ma, *Colloids Surf. B Biointerfaces*, 2015, **136**, 752–760.
5 A. Jaafar, C. Hecker, P. Árki and Y. Joseph, *Bioengineering*, 2020, **7**, 127.
6 D. Chopra, K. Gulati and S. Ivanovski, *Acta Biomater.*, 2021, **127**, 80–101.
7 R. J. Talib and M. R. Toff, *Med. J. Malaysia*, 2004, **59**, 153–154.
8 R. Wang, S. Ni, L. Ma and M. Li, *Front. Bioeng. Biotechnol.*, 2022, **10**, 973297.
9 J. Zhou and L. Zhao, *Acta Biomater.*, 2016, **43**, 358–368.
10 Q. Huang, X. Li, T. A. Elkhooly, X. Liu, R. Zhang, H. Wu, Q. Feng and Y. Liu, *Colloids Surf. B Biointerfaces*, 2018, **170**, 242–250.
11 Z. Zhang, J. Sun, H. Hu, Q. Wang and X. Liu, *J. Biomed. Mater. Res. B Appl. Biomater.*, 2011, **97**, 224–234.
12 E. M. Szesz, G. B. de Souza, G. G. de Lima, B. A. da Silva, N. K. Kuromoto and C. M. Lepienski, *J. Mater. Sci. Mater. Med.*, 2014, **25**, 2265–2275.

13 K. J. Horning, S. W. Caito, K. G. Tipps, A. B. Bowman and M. Aschner, *Annu. Rev. Nutr.*, 2015, **35**, 71–108.
14 Y. Anwar, *Int. J. Biol. Macromol.*, 2018, **111**, 1140–1145.
15 N. Jiang, F. Guo, W. Xu, Z. Zhang, H. Jin, L. Shi, X. Zhang, J. Gao and H. Xu, *Toxicology*, 2020, **436**, 152429.
16 S. Wang, L. Deng, Y. Lv, T. Zhang, X. Zhang, Z. Dong and G. Cai, *Surf. Coating. Technol.*, 2023, **454**, 129197.
17 X. Ni, Q. Zhao, F. Zhou, X. Pan, G. Zhao, X. Zhu, L. Ren, J. Yu, B. Cai and J. Mi, *Mater. Express*, 2022, **12**, 817–822.
18 B. J. Tan, K. J. Klabunde and P. M. A. Sherwood, *J. Am. Chem. Soc.*, 1991, **113**, 855–861.
19 C. d. S. Bezerra and M. E. G. Valerio, *Phys. B Condens. Matter*, 2016, **501**, 106–112.
20 M. Kaur and K. Singh, *Mater. Sci. Eng. C Mater. Biol. Appl.*, 2019, **102**, 844–862.
21 L. Le Guéhennec, A. Soueidan, P. Layrolle and Y. Amouriq, *Dent. Mater.*, 2007, **23**, 844–854.
22 M. Saksø, S. S. Jakobsen, H. Saksø, J. Baas, T. Jakobsen and K. Søballe, *Open Orthop. J.*, 2012, **6**, 376–382.
23 D. D. Bosshardt, V. Chappuis and D. Buser, *Periodontol*, 2017, **73**, 22–40.
24 A. I. Kozelskaya, S. Rutkowski, J. Frueh, A. S. Gogolev, S. G. Chistyakov, S. V. Gnedenkov, S. L. Sinebryukhov, A. Frueh, V. S. Egorkin, E. L. Choynzonov, M. Buldakov, D. E. Kulbakin, E. N. Bolbasov, A. P. Gryaznov, K. N. Verzunova, M. D. Apostolova and S. I. Tverdokhlebov, *J. Funct. Biomater.*, 2022, **13**, 285.
25 W.-H. Song, Y.-K. Jun and S.-H. Hong, Biomimetic apatite coatings on micro-arc oxidized titania, *Biomaterials*, 2004, **25**(17), 3341–3349.
26 C. J. Chung, R. T. Su, H. J. Chu, H. T. Chen, H. K. Tsou and J. L. He, *J. Biomed. Mater. Res. B Appl. Biomater.*, 2013, **101**, 1023–1030.
27 M. M. Shalabi, A. Gortemaker, M. A. Van't Hof, J. A. Jansen and N. H. Creugers, *J. Dent. Res.*, 2006, **85**, 496–500.
28 L. Feller, R. Chandran, R. A. Khammissa, R. Meyerov, Y. Jadwat, M. Bouckaert, I. Schechter and J. Lemmer, *South African Dent. J.*, 2014, **69**(112), 114–117.
29 G. S. Kaliaraj, T. Siva and A. Ramadoss, *J. Mater. Chem. B*, 2021, **9**, 9433–9460.
30 L. Yu, Y. Tian, Y. Qiao and X. Liu, *Colloids Surf. B Biointerfaces*, 2017, **152**, 376–384.
31 Q. Zhao, L. Yi, A. Hu, L. Jiang, L. Hong and J. Dong, *J. Mater. Chem. B*, 2019, **7**, 2284–2299.
32 Y. Li, W. Wang, H. Liu, J. Lei, J. Zhang, H. Zhou and M. Qi, *Mater. Sci. Eng. C Mater. Biol. Appl.*, 2018, **87**, 90–103.
33 Q. M. Zhao, Y. Y. Sun, C. S. Wu, J. Yang, G. F. Bao and Z. M. Cui, *Nanotoxicology*, 2020, **14**, 289–309.
34 C. R. Arciola, D. Campoccia and L. Montanaro, *Nat. Rev. Microbiol.*, 2018, **16**, 397–409.
35 S. Veerachamy, T. Yarlagadda, G. Manivasagam and P. K. Yarlagadda, *Proc. Inst. Mech. Eng. H.*, 2014, **228**, 1083–1099.
36 H. Chouirfa, H. Bouloussa, V. Migonney and C. Falentin-Daudré, *Acta Biomater.*, 2019, **83**, 37–54.
37 L. Yu, S. Qian, Y. Qiao and X. Liu, *J. Mater. Chem. B*, 2014, **2**, 5397–5408.
38 J. Zhou, B. Li and Y. Han, *Sci. Rep.*, 2018, **8**, 17858.
39 C. Yang, Y. Wang and H. Xu, *Biomed. Environ. Sci.*, 2017, **30**, 147–149.